Phase transitions of the anisotropic Dicke model

Pragna Das,[1] Devendra Singh Bhakuni,[2] and Auditya Sharma[1]
[1]*Indian Institute of Science Education and Research Bhopal 462066 India*
[2]*Department of Physics, Ben-Gurion University of the Negev, Beer-Sheva 84105, Israel*

(Received 29 August 2022; revised 6 February 2023; accepted 3 April 2023; published 14 April 2023)

We systematically analyze the various phase transitions of the anisotropic Dicke model that is endowed with both rotating and counterrotating light-matter couplings. In addition to the ground-state quantum phase transition (QPT) from the normal to the superradiant phase, the anisotropic Dicke model also exhibits other transitions, namely, the excited state quantum phase transition (ESQPT), ergodic to nonergodic transition (ENET), and the temperature-dependent phase transition. We show that these phase transitions are profitably studied not only with the standard consecutive level spacing ratio, but also with the aid of various eigenvector quantities such as von Neumann entanglement entropy, the participation ratio, multifractal dimension, and mutual information. For ENET, both the statics and dynamics of the participation ratio offer a consistent and useful picture. An exciting finding from our work is that the ESQPT and the ENET are closely related to each other. We show this with the aid of two characteristic energies in the spectrum corresponding to jumps in von Neumann entropy.

DOI: 10.1103/PhysRevA.107.043706

I. INTRODUCTION

The Dicke model [1–4], which is paradigmatic within the field of cavity quantum electrodynamics, describes the interaction between N atoms and a single-mode bosonic field via a dipole coupling strength. In the thermodynamic limit ($N \to \infty$), the model shows a quantum phase transition from the normal phase (NP) to the superradiant phase (SP) [1,5–10] at some critical coupling strength. Along with this quantum phase transition (QPT), the Dicke model also exhibits two other distinct phase transitions [11], namely, the excited-state quantum phase transition (ESQPT) [6,12–16] and the thermal phase transition (TPT) [17–20]. While the first occurs at finite energy when the coupling strength is sufficiently large, the second, on the other hand, occurs at a finite temperature [18]. Some of these quantum phase transitions were observed experimentally in Bose-Einstein condensates [21] and quantum cavity systems [22]. The physics of systems with light-matter interactions has enjoyed a great deal of interest in recent times, triggered by a number of experimental works [23–25].

A generalized version of the Dicke model, namely, the anisotropic Dicke model [16,26–35] (ADM), where the coupling strengths corresponding to the rotating and counterrotating terms are different, has gained traction in recent times. While a huge body of literature has been built around the Dicke model [8,36–40], the anisotropic model has received relatively less attention. The asymmetry in the coupling brings some novel features in addition to the existing properties of the Dicke model. One such novel feature that has generated considerable excitement is that the ADM not only exhibits the normal to superradiant quantum phase transition, but also an ergodic-to-nonergodic transition (ENET) [31,35]. The model is integrable in the limit where either one of the couplings is zero. Moreover, while the ground-state properties show the normal-to-superradiant phase transition, the excited states show signatures of nonergodicity [35]. It was also argued that the transition from the normal to the superradiant phase is quite different in comparison to the ergodic-to-nonergodic transition [31]. In the present work, focusing on eigenvector properties, we show that the normal-to-superradiant phase transition corresponds to the ground state undergoing a localized-to-multifractal transition. On the other hand, the ergodic-to-nonergodic transition corresponds to the middle excited state undergoing a delocalized-to-multifractal transition.

Phase transitions are often characterized by quantum information tools such as entanglement entropy [2,41–44], mutual information [45–48], and so on. These quantities have proven useful not only to mark a variety of phase transitions [41–44,49–51], but in diverse other contexts [52–54] where quantum correlations have an important role. Moreover, some of these quantities are directly related to experimentally measurable observables and have proven to be useful markers of the phase transitions of the Dicke model [40]. Thus, a study of these quantities in the context of phase transitions is of theoretical interest with potential to connect with experimental work.

In this work, we explore the various phase transitions of the anisotropic Dicke model and their dependence on the asymmetric coupling strengths. First, we study the behavior of the well-known quantum phase transition of the ADM using quantum information measures. With the aid of the ground-state energy, average photon number, inverse participation ratio, and its scaling with the Hilbert-space dimension, we highlight that the normal-to-superradiant phase transition is reminiscent of a localization to multifractal phase transition. Next, we highlight the emergence of the excited-state quantum phase transition and the temperature-dependent phase transition and their dependence on the coupling parameters. While these transitions have been studied extensively for the Dicke model [10,12,18,38,40,55], they are also prominently present in the ADM [31,35]. We study the

temperature-dependent phase transition as a function of the rotating and counterrotating coupling strengths with the aid of an old analytical result [26] for the transition temperature. Similar to the Dicke model [10], we find that mutual information between two spins offers a clear signature of the thermal phase transition, which is benchmarked against the analytical expression for the critical temperature which has already been worked out in the literature [26,30].

Our main result is to show that the ESQPT is profitably studied with the help of von Neumann entanglement entropy between the bosons and the spins, the average level spacing ratio, and two characteristic energies that define a central band in the superradiant phase. With the help of the participation ratio and multifractal dimension, we show that the middle excited state exhibits multifractal behavior in the nonergodic phase. Thus the middle excited state behaves in stark contrast to the ground state, which shows a change from localized to multifractal behavior as one goes from the normal to the superradiant phase. The correspondence between the multifractal nature of the middle excited state and the nonergodic phase is also captured dynamically when we study the participation ratio in a quench dynamical protocol. Another exciting finding of our work is that the excited-state quantum phase transition and the nonergodic-to-ergodic transition are closely related. Specifically, we find that the phase diagram obtained by keeping track of the size of the jumps in von Neumann entropy for the different eigenstates of the system (which carry signatures of the ESQPT), closely resembles the ENET phase diagram. While the ESQPT in the anisotropic Dicke model was explored in Ref. [16], it is mainly focused on the properties of the eigenvalues. The authors of Ref. [32] studied the atom-field and atom-atom entanglement in the anisotropic Dicke model in which the couplings are restricted to $g_1 \geqslant g_2$. Our work considers a more general parameter regime with arbitrary nonnegative g_1 and g_2 like in Buijsman *et al.* [31].

The organization of the paper is as follows. In the Sec. II, we introduce the model Hamiltonian. Next we discuss the various phase transitions (QPT, ESQPT, ENET, TPT) exhibited by the anisotropic Dicke model and their characterization via tools from quantum information theory. While the QPT, ESQPT, and ENET are covered in Sec. III, Sec. IV is dedicated to the TPT. Finally in Sec. V we summarize the main results.

II. MODEL HAMILTONIAN

The Hamiltonian consists of a single-mode bosonic field coupled to N atoms with anisotropic couplings of the rotating and counterrotating terms

$$\mathcal{H} = \omega a^\dagger a + \omega_0 J_z + \frac{g_1}{\sqrt{2j}}(a^\dagger J_- + a J_+) + \frac{g_2}{\sqrt{2j}}(a^\dagger J_+ + a J_-). \tag{1}$$

Here the operators a and $a^\dagger$ are bosonic annihilation and creation operators, respectively, and $J_{\pm,z} = \sum_{i=1}^{2j} \frac{1}{2}\sigma_{\pm,z}^{(i)}$ are angular momentum operators of a pseudospin with length j, composed of $N = 2j$ spin- $\frac{1}{2}$ atoms described by Pauli matrices $\sigma_{\pm,z}^{(i)}$ acting on site i. The commutation relations (in units where $\hbar = 1$) between the various operators are as follows:

$$[a, a^\dagger] = 1, [J_z, J_\pm] = \pm J_\pm, [J_+, J_-] = 2J_z. \tag{2}$$

The basis of the full Hilbert space of the system is $\{|n\rangle \otimes |j, m\rangle\}$ where $|n\rangle$ are the number states of the field satisfying $a^\dagger a|n\rangle = n|n\rangle$ and $|j, m\rangle$ are the Dicke states satisfying $J_\pm|j, m\rangle = \sqrt{j(j+1) - m(m \pm 1)}|j, m \pm 1\rangle$. ω is the single-mode frequency of the bosonic field while ω_0 is the level splitting of the atoms. g_1 and g_2 are the time-independent coupling strengths corresponding to the rotating and counterrotating light-matter interaction terms. In the thermodynamic limit, the system shows a second-order quantum phase transition from normal-to-superradiant phase at $g_1 + g_2 = 1$. For $g_1 + g_2 < 1$, the system is in the normal phase with $\langle a^\dagger a\rangle/j \approx 0$ (the bosonic mode is microscopically excited) and for $g_1 + g_2 > 1$, it is in the superradiant phase with a positive value of $\langle a^\dagger a\rangle/j$ (bosonic mode of the system is macroscopically excited). Here the expectation value is calculated with respect to the ground state of the system Hamiltonian. The ADM possesses a parity symmetry $[H, \Pi] = 0$ with $\Pi = \exp(i\pi[a^\dagger a + J_z + j])$ having eigenvalues ± 1 [31]. Here, we restrict ourselves to the $+1$ eigenvalue and an even atom number N and the symmetric subspace where $j = \frac{N}{2}$. Hence the $(N + 1)$ values that m can take are $(-\frac{N}{2}, \ldots, 0, \ldots, \frac{N}{2})$. For our numerics we truncate the boson number to take the values $n = 0, 1, \ldots, n_{\max}$. Thus the total Hilbert space dimension for the truncated model is $N_D = (n_{\max} + 1)(N + 1)$. We checked that all our numerical results (for the specified $n_{\max}$) are robust against further increase in $n_{\max}$, thus the truncation is carried out in such a way that our numerical results are reliable. Furthermore, we fix $\omega_0 = 1$ as the dimension of energy and the other observables are calculated in units of ω_0.

In the thermodynamic limit (when the number of atoms $N \to \infty$) the model is analytically solvable using the Holstein-Primakoff representation [56,57] of the angular momentum operators $J_z = (b^\dagger b - j)$, $J_+ = b^\dagger\sqrt{2j - b^\dagger b}$, $J_- = J_+^\dagger$. Here b and $b^\dagger$ are bosonic operators that convert the system Hamiltonian into a two-mode bosonic problem. This allows us to obtain effective Hamiltonians that are exact in the thermodynamic limit by neglecting terms from expansions of the Holstein-Primakoff square roots [3]. In the normal phase $g_1 + g_2 < \sqrt{\omega\omega_0}$, the square roots can be expanded directly and the effective Hamiltonian is

$$\mathcal{H}^{(1)} = \omega a^\dagger a + \omega_0(b^\dagger b - j) + g_1(a^\dagger b + a b^\dagger) + g_2(a^\dagger b^\dagger + ab), \tag{3}$$

which is bilinear in the bosonic operators. In this representation, the parity operator Π becomes $\Pi = \exp(i\pi[a^\dagger a + b^\dagger b])$. In the superradiant phase $g_1 + g_2 > \sqrt{\omega\omega_0}$, both the field and the atomic ensemble acquire macroscopic occupations and for that one needs to displace the bosonic modes

$$a^\dagger \to c^\dagger + \sqrt{\alpha}, \quad b^\dagger \to d^\dagger - \sqrt{\beta},$$

where the undetermined parameters α and β are of order $O(j)$. Now considering the thermodynamic limit, the Hamiltonian

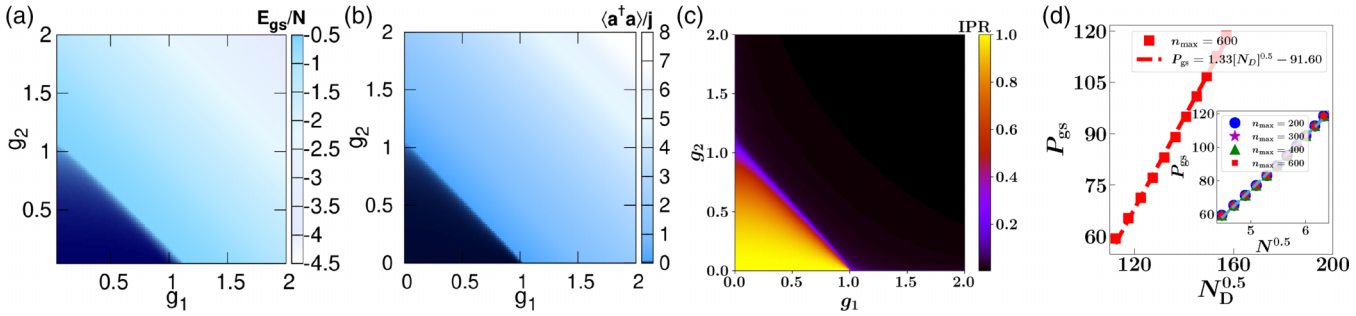

FIG. 1. (a) Ground-state energy of ADM shows NP to SP QPT. (b) Average number of boson (which is scaled by the pseudospin length j) is close to zero for NP ($g_1 + g_2 < 1$) and nonzero for SP ($g_1 + g_2 > 1$). (c) The ground-state IPR is one in NP (localized) and close to zero in the SP (delocalized). (d) Scaling of ground-state *PR* with the full Hilbert space dimension N_D at some point $g_1 = 1.2$, $g_2 = 0.8$, in the SP for ADM for $n_{\max} = 600$ and changing the atom number: $N \in [20, 40]$. PR_{gs} scales as $\sqrt{N_D}$. Here $N_D = (n_{\max} + 1)(N + 1)$ is increasing due to increase of atom number N. In the inset we consider four $n_{\max}$ values: $n_{\max} = 200$ (blue solid circles), 300 (purple stars), 400 (green triangles), 600 (red squares) and changing the atom number: $N \in [20, 40]$. PR_{gs} scales as $\sqrt{N}$. For each fixed $n_{\max}$ dashed lines indicate the fitting with $\sqrt{N}$. The four sets of P_{gs} values overlap. For (a)–(c) the parameters are $\omega = \omega_0 = 1$, $N = 40$. The bosonic cutoff is set to be $n_{\max} = 200$, and this is shown to be large enough. Energy is calculated in units of ω_0 and we fix $\omega_0 = 1$ throughout this paper.

can be written as

$$\mathcal{H}^{(2)} = \omega c^\dagger c + \left[\omega_0 + \frac{(g_1+g_2)}{k}\sqrt{\frac{\alpha\beta k}{2j}}\right] d^\dagger d - \left[(g_1+g_2)\frac{\beta k}{2j} - \omega\sqrt{\alpha}\right](c^\dagger + c) + \left[\frac{2(g_1+g_2)}{k}\sqrt{\frac{\alpha k}{2j}}(j-\beta) - \omega_0\sqrt{\beta}\right]$$
$$\times (d^\dagger + d) + \frac{(g_1+g_2)}{4k^2}\sqrt{\frac{\alpha\beta k}{2j}}(2k+\beta)(d^\dagger + d)^2 + \frac{(g_1+g_2)\beta}{2k}\sqrt{\frac{k}{2j}}(c^\dagger + c)(d^\dagger + d) + \sqrt{\frac{k}{2j}}[g_1(c^\dagger d + cd^\dagger)$$
$$+ g_2(c^\dagger d^\dagger + cd)] + \left[\omega_0(\beta - j) + \omega\alpha - 2\frac{(g_1+g_2)}{k}\sqrt{\frac{\alpha\beta k}{2j}}\right], \tag{4}$$

where $k \equiv 2j - \beta$. This effective Hamiltonian in SP is also bilinear in the bosonic operators. The global symmetry Π is broken at the phase transition and two new local symmetries appear corresponding to the operator $\Pi^{(2)} = \exp(i\pi[c^\dagger c + d^\dagger d])$ [3].

III. QPT, ESQPT, AND ENET

In this section we discuss three types of transitions in the anisotropic Dicke model: QPT, ESQPT, and ENET, in separate subsections. To do the numerics we perform exact diagonalization of the system Hamiltonian. Due to the bosonic mode, the Hilbert space dimension of the ADM is infinite dimensional, however, for numerics one has to truncate the Hilbert space by cutting off the bosonic mode at some finite $n_{\max}$. We checked that our results remain robust on increasing $n_{\max}$ (see the Appendix).

A. Quantum phase transition

In Fig. 1(a) we show the ground-state energy density (energy scaled by the atom number, E_{gs}/N) of the system Hamiltonian as a function of g_1 and g_2. While in the normal phase, the energy is almost constant close to $= -0.5$ (which is very similar to the value seen for the isotropic Dicke model), the superradiant phase has a broad energy spectrum with the density ranging from $-4.5 \leqslant \frac{E_{gs}}{N} \leqslant -0.5$. This clearly distinguishes the normal and superradiant phases. Furthermore, the mean photon number given by the operator $\langle a^\dagger a\rangle/j$ [3] is almost zero in the normal phase, while in the superradiant phase it has a nonzero value with a continuous change across the transition line $g_1 + g_2 = 1$ [Fig. 1(b)] and indicates a second-order phase transition.

Finally, we study the ground-state properties by looking at the degree of localization using the (inverse) participation ratio. The participation ratio [58,59] (PR) of an eigenstate $|\psi\rangle = \sum_j^{N_D} \psi_j|j\rangle$ (where N_D is the Hilbert space dimension) is defined as

$$P = \frac{1}{\sum_{j=1}^{N_D} |\psi_j|^4}. \tag{5}$$

The inverse of the participation ratio, called the inverse participation ratio (IPR $= 1/$PR) is often a useful measure in its own right. From the inset of Fig. 1(c), it is clear that, in the normal phase, IPR is close to unity suggesting that the ground state is localized. On the other hand, a careful study of the scaling of PR in the superradiant phase with the Hilbert-space dimension N_D reveals interesting features. The PR scales as PR $\sim\sqrt{N_D}$ and suggests that the ground state in the superradiant phase exhibits multifractal behavior [see Fig. 1(d)].

In Fig. 1(d) we fix the parameters to be $g_1 = 1.2$, $g_2 = 0.8$ to show a representative example in the SP. While the bosonic cutoff is fixed at $n_{\max} = 600$ we vary the atom number N and hence the total Hilbert space dimension N_D of the truncated model also varies. The change in N_D is entirely due to the change in atom number N since $n_{\max}$ remains fixed. In this figure the red squares are the data for $P_{\rm gs}$ whereas the red dashed line denotes the fit to the functional form $N_D^{0.5}$. In the inset of Fig. 1(d) we choose four different $n_{\max}$ values $n_{\max} = 200$ (blue solid circles), 300 (purple stars), 400 (green triangles), 600 (red squares) and for each fixed $n_{\max}$ we show data as the atom number N (and hence the total Hilbert space dimension N_D) varies exactly like in the main figure. The four sets of data corresponding to different $n_{\max}$ exactly overlap with each other. The dashed lines denote the data fitting of $P_{\rm gs}$ with $N^{0.5}$. Hence we can conclude that for a fixed atom number N, $P_{\rm gs}$ is independent of $n_{\max}$ and only depends on N.

B. Excited state quantum phase transition

We now look at the properties of the excited states and find that similar to the Dicke model, the anisotropic Dicke model also exhibits an excited-state quantum phase transition in the superradiant phase (for $g_1 + g_2 > 1$). While the literature on ESQPT has mainly considered eigenvalue properties [12–15,38,40,60], we showed in our recent paper [10] the profitability of studying eigenvector properties such as the von Neumann entanglement entropy [2], the average bosonic number [3], concurrence [61,62], and participation ratio [58,59]. We also aruged that there is not only a lower cutoff energy but also an upper cutoff and energies between these two cutoffs behave differently from the upper and lower bands. In the Dicke model, the lower cutoff energy [40,60] is the ground-state energy at the critical coupling strength g_c and the upper cutoff energy [10] is the maximum energy at $g = 0$ (for finite $n_{\max}$). On the other hand, in the ADM, we find that the lower cutoff energy is around the ground-state energy of the system on the critical line of quantum phase transitions ($g_1 + g_2 = 1$) while the upper cutoff energy is the maximum energy at $g_1 = g_2 = 0$ (for finite $n_{\max}$). Energies below (above) the lower (upper) cutoff form the lower (upper) energy band and the energies in between the two cutoffs form the central band.

The entanglement entropy between the spins and the bosons is simply the von Neumann entropy of the reduced density matrix of the spins

$$S_{\rm spins} = -{\rm Tr}[\rho_{\rm spins} \ln(\rho_{\rm spins})], \tag{6}$$

where $\rho_{\rm spins}$ is the reduced density matrix of the spins obtained by tracing over the bosonic degrees of freedom. In Fig. 2(a) we show the von Neumann entanglement entropy (between spins and bosons) as a function of the energy eigenvalues at some point $g_1 = 1.0$ and $g_2 = 1.1$. We observe from this representative plot that there are three characteristic parts: (i) an increasing part up to some energy, followed by (ii) a plateau region and then (iii) a region where VNEE decreases. To quantify the beginning and the end of the plateau region, we define two characteristic energies $E_{\rm lower}$ and $E_{\rm upper}$ as

$$E_{\rm lower} = \left[\frac{\sum_{n=0}^{\frac{N_D}{2}} E_n |\Delta S_n|}{\sum_{n=0}^{\frac{N_D}{2}} |\Delta S_n|} \right], \tag{7}$$

and

$$E_{\rm upper} = \left[\frac{\sum_{n=\frac{N_D}{2}}^{N_D} E_n |\Delta S_n|}{\sum_{n=\frac{N_D}{2}}^{N_D} |\Delta S_n|} \right], \tag{8}$$

where $\Delta S_n = S_{n+1} - S_n$ is the VNEE difference between that of the $(n+1)$th eigenstate and the nth eigenstate, and E_n is the nth energy. The above energies are obtained by using the jumps in the VNEE as weights. The change in VNEE is taken as weights for the different energies, and we would thus expect these quantities to signal the two ends of the plateau region. In Fig. 2(a), these two energies are marked by two vertical lines: the orange dash-dotted line denotes $E_{\rm lower}$ whereas the blue dashed line denotes $E_{\rm upper}$ and they more or less match with the two end energies of the plateau region. Now we define two more new quantities, $\chi_{\rm lower}$ and $\chi_{\rm upper}$:

$$\chi_{\rm lower} = \frac{E_{\rm lower}}{E^0_{\rm normal}}, \tag{9}$$

$$\chi_{\rm upper} = \frac{E_{\rm upper}}{E^{\rm max}_{g_1,g_2=0}}, \tag{10}$$

where $E^0_{\rm normal}$ is the minimum energy in the normal phase ($g_1 + g_2 < 1$) and $E^{\rm max}_{g_1,g_2=0}$ is the maximum energy at $g_1 = g_2 = 0$ (for finite $n_{\max}$). We plotted these two quantities as a function of g_1 and g_2 in Figs. 2(b) and 2(c). Remarkably this reveals a clear visual correlation between the ESQPT and what is called the ergodic-to-nonergodic phase transition (ENET) [31], which we describe in greater detail in the following subsection. Moreover we notice that, along the diagonal line [it is more clear in Fig. 2(c)] there is a relatively dark line which indicates that the symmetric Dicke model is special. A quantitative way of identifying the central band of energies corresponding to the plateau region in Fig. 2(a) is to consider the energies that lie between $\chi_{\rm lower} = 1$ and $\chi_{\rm upper} = 1$, i.e., $E_{\rm lower} = E^0_{\rm normal}$ and $E_{\rm upper} = E^{\rm max}_{g_1,g_2=0}$. We perform a study of the average level spacing ratio [63] $\langle r \rangle$ for the energies lying between $E_{\rm lower}$ and $E_{\rm upper}$. Let s_n denote the level spacing between two consecutive energies E_{n+1} and E_n, then the $\langle r \rangle$ is defined as the average over n of the ratio of consecutive level spacings

$$r_n = \frac{\min(s_{n-1},\ s_n)}{\max(s_{n-1},\ s_n)}. \tag{11}$$

For an ergodic system, the value of $\langle r \rangle = 0.53$ and the probability distribution of the consecutive gaps shows Wigner-Dyson statistics [64] while for a nonergodic system it is $\langle r \rangle = 0.386$ and the probability distribution becomes Poissonian.

Figure 2(d) shows the phase diagram based on the level spacing ratio. It can be seen that a small value of either g_1 or g_2 leads to a nonegrodic phase where the eigenvalue statistics obey the Poisson distribution with $\langle r \rangle \approx 0.386$. On the other hand, when both the couplings are significantly large, we see

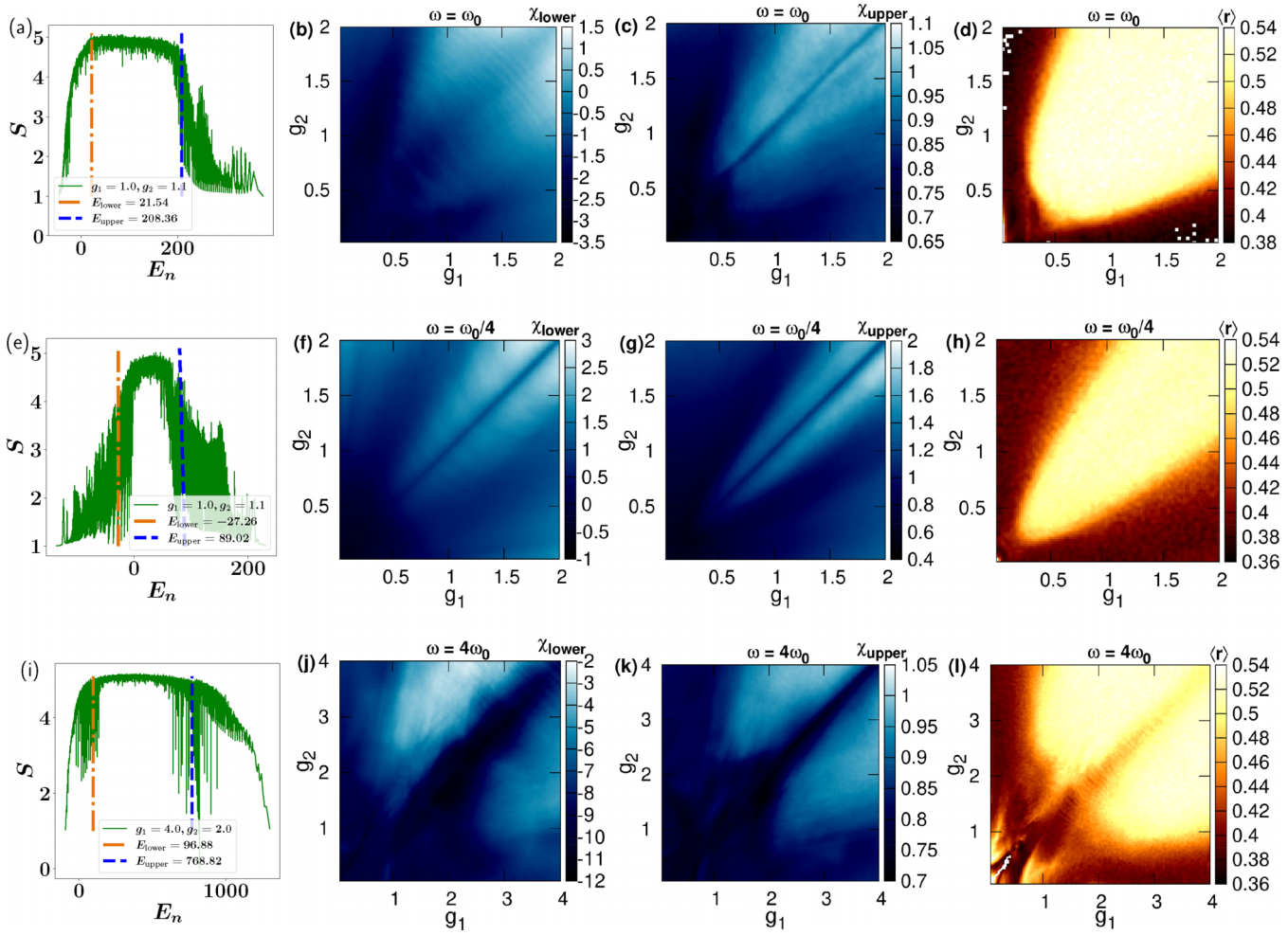

FIG. 2. (a), (e), and (i) Von Neumann entanglement entropy as a function of the eigenstate energies of the ADM Hamiltonian at the point $g_1 = 1.0,\ g_2 = 1.1$ [for (a) and (e)] and at the point $g_1 = 4,\ g_2 = 2$ [for (i)]. In the figure the orange dash-dotted line denotes E_{lower} [given in Eq. (7)] and the blue dashed line is for E_{upper} [given in Eq. (8)]. (b), (f), and (j) χ_{lower} [given in Eq. (9)] as a function of g_1 and g_2. (c), (g), and (k) χ_{upper} [given in Eq. (10)] as a function of g_1 and g_2. (b,c) show similar phase transition from nonergodic to ergodic phase, which suggest that ESQPT is related to ENET. (d), (h), and (l) Consecutive level spacing ratio $\langle r\rangle$ of the energies lying between E^0_{normal}, $E^{\max}_{g_1,g_2=0}$. For all the above figures atom number $N = 40$ and we take the bosonic cutoff $n_{\max} = 200$. Top panel is for resonant case $\omega = \omega_0 = 1$, middle and bottom panels are for two off-resonant cases $\omega = \frac{\omega_0}{4}$ and $\omega = 4\omega_0$, respectively.

a crossover to Wigner-Dyson distribution where the level-spacing ratio becomes $\langle r\rangle \approx 0.53$. It is worth mentioning that this nonergodic-to-ergodic transition is quite different from the normal to superradiant phase transition. We perform a careful analysis of this phase transition in the next subsection. We show that the Wigner-Dyson behavior corresponds to the energy band that lies between the two cutoffs [10] ($E_{\text{lower}} = E^0_{\text{normal}}$, $E_{\text{upper}} = E^{\max}_{g_1,g_2=0}$).

So far we restricted ourselves to the resonant case $\omega = \omega_0$. Now we also study ESQPT for the off-resonant cases considering $\omega = \frac{\omega_0}{4}$ (middle panel of Fig. 2) and $\omega = 4\omega_0$ (bottom panel of Fig. 2). Studying the consecutive level spacing ratio of the energy band sandwiched between E^0_{normal} and $E^{\max}_{g_1,g_2=0}$ [see Figs. 2(h) and 2(l)], we see a transition from $\langle r\rangle \approx 0.386$ to $\langle r\rangle \approx 0.53$ that is a nonergodic-to-ergodic transition. From a careful observation of Figs. 2(f) and 2(g) and 2(j) and 2(k) we infer that while a clear correspondence between ENET and ESQPT is present for $g_1 \neq g_2$ even in the off-resonant scenario, the diagonal direction ($g_1 = g_2$) corresponding to the Dicke model exhibits special behavior [6].

C. Ergodic to nonergodic transition

1. Statics

As discussed in the previous subsection, different eigenstates play a role in different phase transitions. While the ground state shows the normal-to-superradiant phase transition or equivalently from a localized phase to a multifractal phase, the middle excited states exhibit a nonergodic-to-ergodic transition. Here, we study the phase diagram on the g_1, g_2 plane of the ADM for different eigenstates with the help of participation ratio and multifractal dimension and explore the possibility of multifractal states in the excited states.

While the participation ratio quantifies the degree of localization and delocalization of a quantum state, a study of its scaling with the system size offers further insights. When the

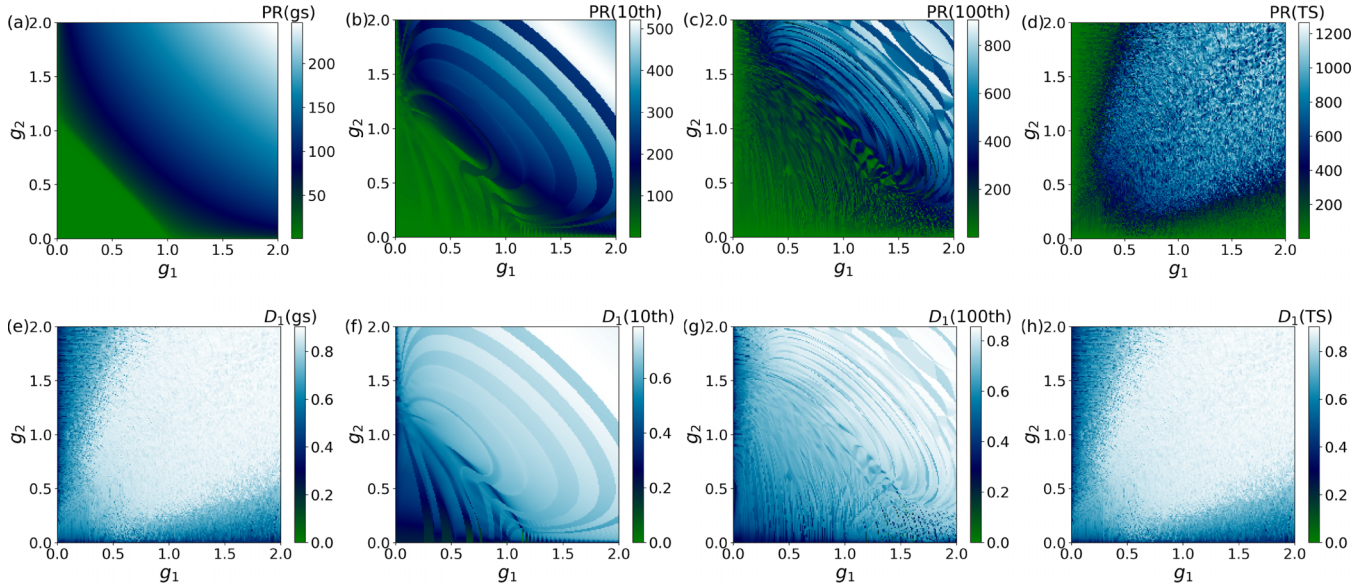

FIG. 3. Participation ratio and multifractal dimension, D_1 of ADM for different eigenstate of the system Hamiltonian as a function of coupling parameters g_1 and g_2. (a)–(d) are the figure for participation ratio corresponding to ground state (gs), tenth excited state, 100th excited state, and middle excited state or thermal state (TS), respectively. (e) D_1 for the ground state shows QPT from localization (NP) to multifractal (SP) behavior. (f) D_1 for the tenth excited state. (g) D_1 for the 100th excited state. (h) D_1 for the middle excited state shows ENET from nonergodic extended (multifractal) to ergodic (delocalized) behavior. For all the above plots parameters are $\omega = \omega_0 = 1$, atom number $N = 40$. We take the bosonic cutoff to be $n_{\max} = 200$.

Hilbert space dimension is large (N_D is large) the multifractal dimension [65,66] can be represented as

$$D_q = \frac{1}{1-q}\frac{\ln\left(\sum_{j=1}^{N_D}|\psi_j|^{2q}\right)}{\ln(N_D)}, \tag{12}$$

where $|\psi\rangle$ is an eigenstate of the Hamiltonian and $S_q = \frac{1}{1-q}\ln\left(\sum_{j=1}^{N_D}|\psi_j|^{2q}\right)$ is known as the q-dependent participation entropy. In the Shannon limit, $S_1 = -\sum_j |\psi_j|^2 \ln(|\psi_j|^2)$, while the $q = 2$ participation entropy is connected to the usual participation ratio as $S_2 = \ln(P)$. For a perfectly delocalized state $S_q = \ln(N_D)$, (when N_D is large) and hence $D_q = O(1)$, for all q. On the other hand, for a localized state $S_q =$ constant and $D_q = 0$. In an intermediate situation, wave functions are extended but nonergodic with $S_q = D_q \ln(N_D)$ where $0 < D_q < 1$ and the state is multifractal in that particular basis.

In Fig. 3 we show the phase diagrams of the ADM based on participation ratio [Figs. 3(a) to 3(d)] and the multifractal dimension D_1 [Figs. 3(e) to 3(h)] for different eigenstates of the system Hamiltonian. For a fixed system size, we pick a few states including the ground state and the middle excited state. While for the ground state, we clearly see the normal-to-superradiant phase transition along the line $g_1 + g_2 = 1$ as shown by the phase diagram of the participation ratio [Fig. 1(d)] and the multifractal dimension [Fig. 3(e)], as the states become more and more excited, it is the nonergodic-to-ergodic transition that is highlighted. Studying the PR of the middle excited state [Fig. 3(d)], we see a similar phase diagram as that of the level spacing ratio of the system as a function of g_1 and g_2 [see Fig. 2(d)], signifying a transition from the nonergodic phase to the ergodic phase. In the nonergodic phase the PR value is low whereas in the ergodic phase its value is relatively higher.

In Figs. 3(e) to 3(h) we study the multifractal dimension D_1 for the different eigenstates of the ADM as a function of coupling parameters g_1 and g_2 similar to the participation ratio. Here in Fig. 3(e) we show the nature of D_1, for the ADM ground state. In the NP, $D_q \approx 0$ whereas in the SP, $0 < D_1 < 1$. This suggests a transition from a localized to a multifractal phase. Figure 3(h) shows D_1 for the middle excited state of the ADM. In this figure we see the regions (depicted by the blue color) where $0 < D_1 < 1$ which behaves like a multifractal phase, whereas the region where $D_1 \approx 0.9$ (depicted by the white color), behaves as more like a delocalized phase. Hence the middle excited state shows a transition from an extended nonergodic (multifractal) phase to an ergodic (delocalized) phase.

2. Dynamics

To study the quench dynamics of a closed quantum system, one prepares the system in some eigenstate of the initial Hamiltonian $\mathcal{H}_0$. The Hamiltonian is suddenly changed to $\mathcal{H} = \mathcal{H}_0 + \mathcal{H}_1$ and the system is allowed to evolve under the corresponding unitary time evolution operator. Here, we take the middle excited state of the decoupled Hamiltonian ($\mathcal{H}_0 = \omega a^\dagger a + \omega_0 J_z$) as our initial state, which can be written as $|\psi_{\text{in}}\rangle = \sum_\alpha C_\alpha |\alpha\rangle$, with $|\alpha\rangle = |n, j, m\rangle$ being a computational basis state and C_α being the corresponding coefficient. The time-evolution of the state is given by $|\psi_t\rangle = e^{-i\mathcal{H}t}|\psi_{\text{in}}\rangle = \sum_\alpha C_\alpha(t)|\alpha\rangle$, where $\mathcal{H}$ is the ADM Hamiltonian. To study the dynamical properties, we calculate the dynamics of the participation ratio $\text{PR}(t) = 1/\sum_\alpha |C_\alpha(t)|^4$ at different times

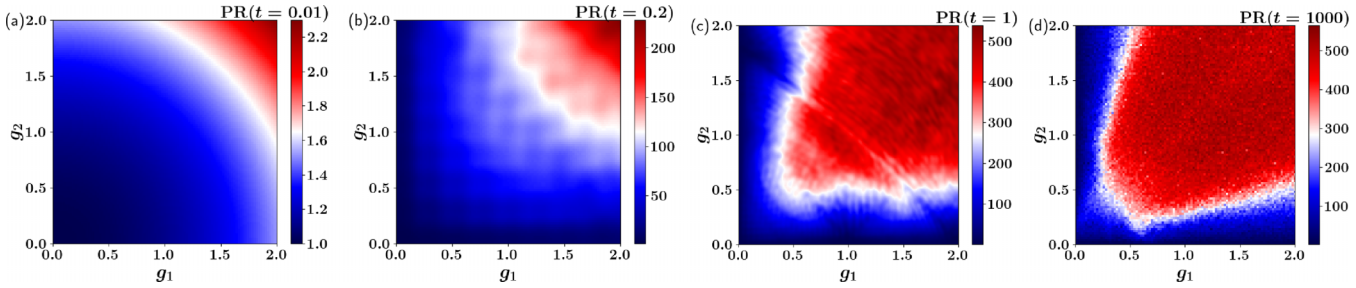

FIG. 4. (a) Quench dynamics of participation ratio of ADM for $\omega = \omega_0 = 1$, $N = 20$, and $n_{\max} = 100$, at different times (a) $t = 0.01$, (b) $t = 0.2$, (c) $t = 1$, (d) $t = 1000$. Here the initial state is the middle excited state of the decoupled Hamiltonian of the system ($H_0 = \omega a^\dagger a + \omega_0 J_z$). The time t is in units of ω_0^{-1} and we fix $\omega_0 = 1$ throughout this paper.

$t = 0.01, 0.2, 1, 1000$. From Fig. 4(a) we see that, for a very small duration of time, say $t = 0.01$, the participation ratio has low value for all g_1 and g_2. As we evolve the system a bit, say at $t = 0.2$, in Fig. 4(b), one can notice that in the red part, the PR value is increasing, for higher values of g_1 and g_2. In fact, this portion in the central region increases with time also. In Fig. 4(c) we see that in the red part the value of PR is significantly higher than in the blue part. When the dynamics is carried out over a very long time [say $t = 1000$ as in Fig. 4(d)], we get a phase diagram which exactly looks like the nonergodic (blue color) to ergodic (red color) phase diagram [see Figs. 4(d) and 3(d)]. Figure 4(d) suggests that, if the system is initially in the nonergodic phase and we evolve it for a long time, the system will stay in the nonergodic phase, i.e., the participation ratio is relatively low no matter how long the time is. This is in contrast to the ergodic phase where the PR value is higher for long times even if the inital PR is low.

IV. THERMAL PHASE TRANSITION

Another type of phase transition exhibited by the ADM is the finite-temperature phase transition [26]. As with the Dicke model, it is known that a finite critical temperature can destroy the superradiant phase and a transition back to the normal phase is obtained going beyond the critical temperature [26]. We can derive an exact analytical expression for the transition temperature as a function of the parameters g_1 and g_2. We start by rewriting the Hamiltonian (in units of ω) as

$$\tilde{\mathcal{H}} = \frac{\mathcal{H}}{\omega} = a^\dagger a + \sum_{j=1}^{N} \frac{\epsilon}{2}\sigma_j^z + \frac{\lambda_1}{2\sqrt{N}} \sum_{j=1}^{N} (a\sigma_j^+ + a^\dagger \sigma_j^-) + \frac{\lambda_2}{2\sqrt{N}} \sum_{j=1}^{N} (a^\dagger \sigma_j^+ + a\sigma_j^-), \tag{13}$$

where $\epsilon = \frac{\omega_0}{\omega}, \lambda_1 = \frac{g_1}{\omega}, \lambda_2 = \frac{g_2}{\omega}$. The partition function for the full ADM is given by

$$Z(N,T) = \sum_{s_1,\ldots,s_N=\pm 1} \int \frac{d^2\alpha}{\pi} \langle s_1, \ldots, s_N | \langle \alpha | e^{-\beta \tilde{\mathcal{H}}} | \alpha \rangle | s_1, \ldots, s_N \rangle. \tag{14}$$

The expectation value of the Hamiltonian with respect to the bosonic modes is

$$\langle \alpha | \tilde{\mathcal{H}} | \alpha \rangle = \alpha^* \alpha + \sum_{j=1}^{N} \left[\frac{\epsilon}{2}\sigma_j^z + \frac{\lambda_1}{2\sqrt{N}} (\alpha \sigma_j^+ + \alpha^* \sigma_j^-) + \frac{\lambda_2}{2\sqrt{N}} (\alpha^* \sigma_j^+ + \alpha \sigma_j^-) \right]. \tag{15}$$

Defining

$$h_j = \frac{\epsilon}{2}\sigma_j^z + \frac{\lambda_1}{2\sqrt{N}} (\alpha \sigma_j^+ + \alpha^* \sigma_j^-) + \frac{\lambda_2}{2\sqrt{N}} (\alpha^* \sigma_j^+ + \alpha \sigma_j^-) \tag{16}$$

the expectation value with respect to the spins becomes a product of single-spin expectation values

$$\langle s_1, \ldots, s_N | \langle \alpha | e^{-\beta \tilde{\mathcal{H}}} | \alpha \rangle | s_1, \ldots, s_N \rangle = e^{-\beta |\alpha|^2} \Pi_{j=1}^{N} \langle s_j | e^{-\beta h_j} | s_j \rangle. \tag{17}$$

Thus the computation of the partition function reduces to the evaluation of a double integral

$$Z(N,T) = \int \frac{d^2\alpha}{\pi} e^{-\beta|\alpha|^2} [\mathrm{Tr} e^{-\beta h}]^N = \int \frac{d^2\alpha}{\pi} e^{-\beta|\alpha|^2} \times \left(2\cosh \left[\frac{\beta\epsilon}{2} \left[1 + \frac{4(\lambda_1+\lambda_2)^2\alpha^2}{\epsilon^2 N} \right]^{1/2} \right] \right)^N, \tag{18}$$

which in the thermodynamic limit ($N \to \infty$) can be solved using the method of steepest descent within the superradiant phase. Tracking the point at which the method breaks down (see the Appendix), we have an exact expression for the transition temperature

$$T_c = \frac{1}{\beta_c} = \left(\frac{\omega_0}{2\omega} \right) \frac{1}{\tanh^{-1}\left(\frac{\omega\omega_0}{(g_1+g_2)^2} \right)}. \tag{19}$$

Thus, in the superradiant phase ($g_1 + g_2 > 1$ at $T = 0$), raising the temperature to a value larger than the critical temperature (T_c), causes the system to go back to the normal phase. We now provide numerical evidence of this phase

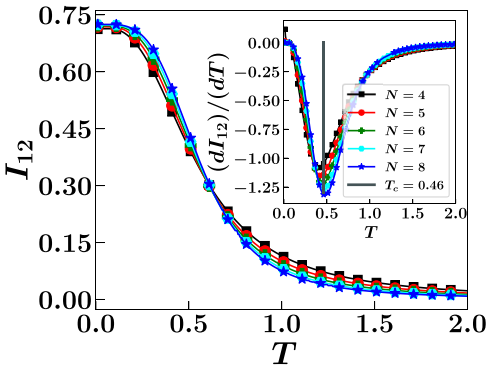

FIG. 5. Mutual information of two spins I_{12} as a function of temperature. Inset of the figure shows the numerical differentiation of MI with respect to temperature $\frac{dI_{12}}{dT}$, at $g_1 = 1.0$, $g_2 = 0.5$. The vertical line represents the theoretical value of the critical temperature $T_c \approx 0.46$. Here $\omega = \omega_0 = 1$, $n_{\max} = 40$.

transition with the help of mutual information between two spins. While the entanglement entropy is a good measure to capture a QPT, it is unsuitable for a TPT since mixed states are involved. Mutual information [45–48] between two spins is a good measure to capture the TPT, as we showed in an earlier work for the Dicke model [10]. We show here that the usefulness of mutual information as a marker of the thermal phase transition extends to the ADM.

When the overall state is mixed, the correlations between two subsystems can be quantified with the help of the mutual information defined as

$$I_{12} = S_1 + S_2 - S_{12}, \tag{20}$$

where $S_{1,2} = -\mathrm{Tr}[\rho_{1,2}\ln(\rho_{1,2})]$, $S_{12} = -\mathrm{Tr}[\rho_{12}\ln(\rho_{12})]$. Here ρ_1, ρ_2 are the reduced density matrices for the two subsystems, S_1, S_2 are the corresponding von Neumann entropies, ρ_{12} is the density matrix of the overall system, and S_{12} is the corresponding entropy. When the overall state is in a pure state, $S_{12} = 0$ and the mutual information become twice the entanglement entropy since $S_1 = S_2$. For our model we study the mutual information between any two spins (due to the symmetry of the system Hamiltonian, it does not matter which spin pair is chosen). Here we use the spin product space, hence we have to diagonalize the system Hamiltonian with dimension $(n_{\max} + 1)2^N$. To calculate I_{12}, we have to take a partial trace of the total density matrix over the bosonic part first and then over the $N - 2$ atoms.

Figure 5 shows the mutual information between two spins. For the parameters $g_1 = 1.0, g_2 = 0.5$, the system is in the superradiant phase at zero temperature where the value of mutual information takes significantly large values (Fig. 5). On increasing the temperature, we see that the mutual information starts to decrease, signifying a change in the direction of the normal phase. To check that mutual information does indeed capture the exact transition between the superradiant-to-normal phase, we plot the derivative of the mutual information with respect to the temperature $\frac{dI_{12}}{dT}$ (inset of the Fig. 5). We observe that the temperature at which the derivative is minimum corresponds to the transition temperature of the TPT from SP to NP for $g_1 + g_2 > 1$. For this particular choice of g_1 and g_2, the critical temperature is $T_c = 0.46$, which we denote by the vertical straight line in the inset figure.

In Fig. 6 we showed I_{12} as a function of g_1 and g_2 at different temperatures: $T = 0$, 0.1, 1.0, and 1.5. Figure 6(a) ($T = 0$) shows a clear QPT from NP (black color) to SP (white color) along the line $g_1 + g_2 = 1$. We emphasize that at zero temperature, the ground state is a pure state, and so the mutual information is really the same as twice the entanglement entropy. I_{12} is close to zero in the normal phase and close to unity in the superradiant phase. Another way of saying this is that the total correlation between two spins is almost zero in the normal phase whereas it is maximum in the superradiant phase. Hence the QPT in the anisotropic Dicke model is similar to the isotropic Dicke model (for which $g_1 = g_2$) but here an additional parameter is introduced. On the other hand, one can notice that as temperature increases [in Figs. 6(b) ($T = 0.1$), 6(c) ($T = 1$), and 6(d) ($T = 1.5$)] the region corresponding to the NP (black portion) also expands: the phase boundary is highlighted by a red dashed line ($g_1 + g_2 =$ constant) which depends on the temperature. Using Eq. (19) we see that for $T = 0.1$, 1, and 1.5, the phase boundary is given by $g_1 + g_2 = 1.01$, $g_1 + g_2 = 2.16$, and $g_1 + g_2 = 2.64$, respectively; beyond the phase boundary, the system is in the SP where the correlation between two spins is close to unity. These

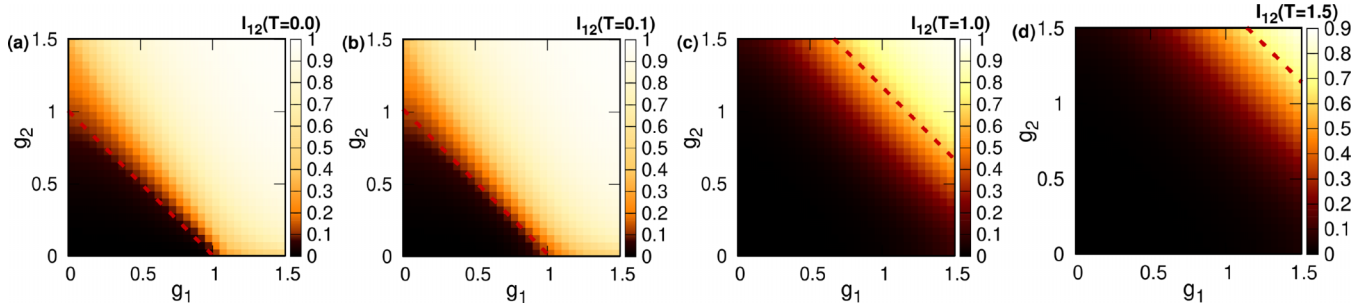

FIG. 6. Mutual information between two spins as a function of g_1 and g_2 at different temperature: (a) $T = 0$ (QPT), (b) $T = 0.1$, (c) $T = 1.0$, (d) $T = 1.5$. As temperature increases, the region corresponding to the normal phase (denoted by black color) also increases. The red dashed line denotes the value of $g_1 + g_2$ for a fixed temperature following Eq. (19). Zero-temperature case denotes QPT along the line $g_1 + g_2 = 1$, for $T = 0.1$, 1 and 1.5, $g_1 + g_2 = 1.01$, 2.16, 2.63, respectively. The parameters are $\omega = \omega_0 = 1$, $N = 6$. The bosonic cutoff is taken to be $n_{\max} = 40$.

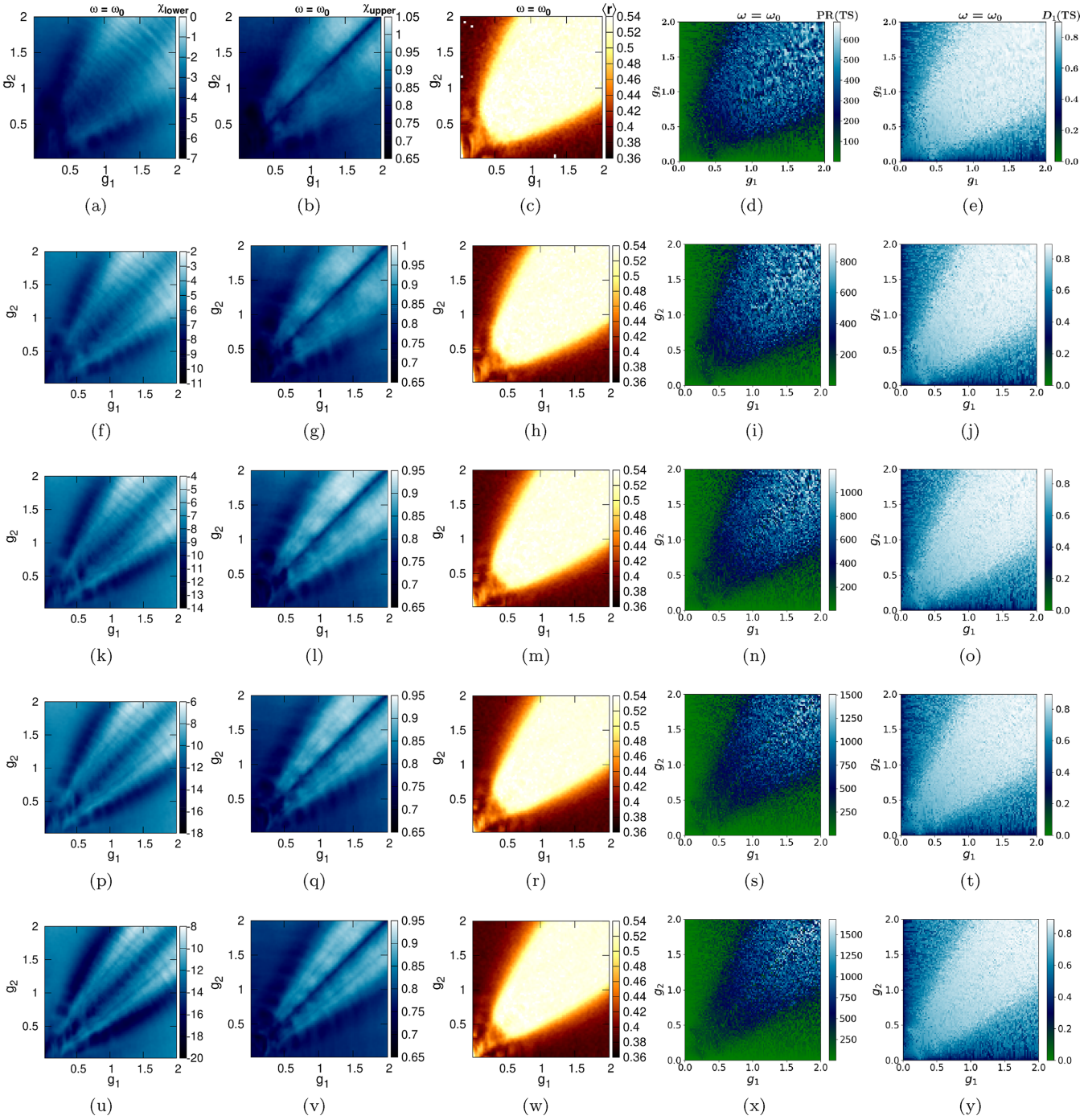

FIG. 7. (a), (f), (k), (p), and (u) χ_{lower} [given in Eq. (9)], (b), (g), (l), (q), and (v) χ_{upper} [given in Eq. (10)], (c), (h), (m), (r), and (w) average consecutive level spacing ratio $\langle r \rangle$; (d), (i), (n), (s), and (x) participation ratio (PR) and (e), (j), (o), (t), and (y) the multifractal dimension D_1 for the middle excited state of the system for the resonance condition ($\omega = \omega_0 = 1$) considering 20 spins and truncating the bosonic mode at gradually increasing values: $n_{\max} = 200,\ 300,\ 400,\ 500,\ 600$ (panels 1 to 5, respectively).

figures indicate that the mutual information between spins is an excellent measure of the thermal phase transition of the system.

V. SUMMARY AND CONCLUSION

We first discuss the ground-state phase transition from a normal phase to the superradiant phase showing that a critical line $g_1 + g_2 = 1$ separates the two phases. We see that the ground-state energy density is almost constant in the NP whereas in the SP we find a broad range of energy densities, which are lower than that in the normal phase. The ground-state number operator is almost zero in the NP while it is nonzero in the SP, indicating macroscopic excitations in the bosonic mode. By studying the participation ratio, we conclude that the ground state of the system exhibits multifractal features in the superradiant phase with the participation ratio scaling as $\text{PR}_{\text{gs}} \propto \sqrt{N_D}$.

Next, we explore the excited state features and find that the ADM also exhibits the excited state phase transition both for the resonant ($\omega = \omega_0$) and the off-resonant ($\omega \neq \omega_0$) cases. The ESQPT is nicely captured by the von Neumann entanglement entropy (between spins and bosons) as a function of eigenstate energies. We observe that for the ADM there exist two cutoff energies separating the different phases: a lower cutoff energy (corresponding to the ground-state energy along the line, $g_1 + g_2 = 1$) and an upper cutoff energy (corresponding to the maximum energy at $g_1 = g_2 = 0$ for finite $n_{\max}$). Between these two cutoff energies, we find that the level statistics exhibits either Poisson statistics or Wigner-Dyson statistics depending on the values of the coupling parameters g_1 and g_2 suggesting a nonergodic-to-ergodic phase transition. A study of the consecutive level spacing ratio of the system for the middle energy band (energy band between the lower and the upper cutoff energies) supports these findings. It is convenient to introduce two new quantities (having the dimensions of energy) that correspond to the lower and upper cutoff energies of the spectrum in the superradiant phase. The above energies are obtained by using the jumps in the VNEE as weights. These characteristic energies, which are a measure of the energies at which the corresponding von Neumman entropies of the eigenstates begin and end their plateau-like behavior, signal the ESQPT of this model. Remarkably, when a phase diagram is obtained using these characteristic energies, we get a picture that looks very similar to the phase diagram obtained using level spacing ratios. Thus from our study, we conclude that the ESQPT and ENET are intimately related to each other for the anisotropic Dicke model ($g_1 \neq g_2$). We checked that this connection is robust both for the resonant ($\omega = \omega_0$) and off-resonant ($\omega \neq \omega_0$) cases for the generic ADM; the diagonal direction ($g_1 = g_2$) corresponds to the Dicke model exhibits special behavior [6]. From a study of eigenstate properties with the aid of participation ratio and multifractal dimension D_1, we see that the normal-to-super-radiant phase transition corresponds to the ground state undergoing a localized-to-multifractal transition. On the other hand, the ergodic-to-nonergodic transition corresponds to the middle excited state undergoing a delocalized-to-multifractal transition. The correspondence between the multifractal nature of the middle excited state and the nonergodic phase is also captured dynamically when we study participation ratio in a quench dynamical protocol.

Finally, the ADM also exhibits yet another phase transition, namely the temperature-dependent phase transition. For $g_1 + g_2 > 1$, there exists a critical temperature, T_c above which the superradiant phase disappears and the system comes back to the normal phase. Following the old work of Hioe [26], we write down an analytical expression for T_c as a function of g_1, g_2. We show that the mutual information between two spins as a function of temperature proves handy to obtain an independent characterization of the thermal phase transition. A study of the mutual information suggests that for $g_1 + g_2 < 1$, the system lies in the normal phase for all temperatures with a relatively lower value of mutual information, but for $g_1 + g_2 > 1$ there exists a T_c such that when $T < T_c$ the system lies in the SP with a relatively higher value of mutual information and for $T > T_c$ the system goes back to NP, showing a temperature-dependent phase transition.

ACKNOWLEDGMENTS

We are grateful to the High Performance Computing (HPC) facility at IISER Bhopal, where the large-scale calculations in this project were run. P.D. is grateful to IISERB for the Ph.D. fellowship. A.S. acknowledges financial support from SERB via Grant No. CRG/2019/003447 and from DST via the DST-INSPIRE Faculty Award No. DST/INSPIRE/04/2014/002461.

APPENDIX A: EXPRESSION FOR THE CRITICAL TEMPERATURE FOR THE TPT

In this Appendix we include a brief derivation of the expression for the critical temperature for TPT similar to the previous work [26]. We begin by recalling the expression of the partition function in the form of a double integral [Eq. (18)]

$$\begin{aligned} Z(N,T) &= \int \frac{d^2\alpha}{\pi} e^{-\beta|\alpha|^2} [\mathrm{Tr} e^{-\beta h}]^N \\ &= \int \frac{d^2\alpha}{\pi} e^{-\beta|\alpha|^2} \\ &\quad \times \left(2\cosh\left[\frac{\beta\epsilon}{2}\left[1+\frac{4(\lambda_1+\lambda_2)^2\alpha^2}{\epsilon^2 N}\right]^{1/2}\right]\right)^N. \end{aligned} \tag{A1}$$

Rewriting the double integral using polar coordinates and defining $y = \frac{r^2}{N}$ and

$$\phi(y) = -\beta y + \ln\left(2\cosh\left[\frac{\beta\epsilon}{2}\left[1+\frac{4(\lambda_1+\lambda_2)^2 y}{\epsilon^2}\right]^{1/2}\right]\right) \tag{A2}$$

we can write

$$Z(N,T) = N\int_0^\infty dy \exp\left[N\phi(y)\right]. \tag{A3}$$

Since we are interested in the thermodynamic limit where $N \to \infty$, we can invoke Laplace's method [67] to evaluate the integral as

$$Z(N,T) = N\frac{C}{\sqrt{N}} \max_{0\leqslant y\leqslant\infty} \exp(N[\phi(y)]), \tag{A4}$$

where C is some constant. To find the maximum of the function $\phi(y)$, we compute its derivative

$$\phi' = -\beta + \frac{\beta(\lambda_1+\lambda_2)^2}{\epsilon}\frac{1}{\eta}\tanh\left(\frac{\beta\epsilon\eta}{2}\right), \tag{A5}$$

where

$$\eta = \left[1+\frac{4(\lambda_1+\lambda_2)^2 y}{\epsilon^2}\right]^{1/2}. \tag{A6}$$

Putting

$$\phi' = 0, \tag{A7}$$

we have

$$\frac{\epsilon\eta}{(\lambda_1+\lambda_2)^2} = \tanh\left(\frac{\beta\epsilon\eta}{2}\right). \tag{A8}$$

The hyperbolic tangent funtion is a monotonically increasing function and is bounded above by unity. Since $\eta \geqslant 1$ by definition [Eq. (A6)], if $(\lambda_1 + \lambda_2)^2 < \epsilon$, there is no solution for Eq. (A8). On the other hand, for $(\lambda_1 + \lambda_2)^2 > \epsilon$, the solution depends on the value of β. The critical value of the inverse temperature β_c can be computed by putting $\eta = 1$ and is given by

$$\beta_c = \frac{2}{\epsilon} \tanh^{-1}\left(\frac{\epsilon}{(\lambda_1 + \lambda_2)^2}\right). \tag{A9}$$

Substituting $\epsilon = \frac{\omega_0}{\omega}$ and $\lambda_1 = \frac{g_1}{\omega}$, $\lambda_2 = \frac{g_2}{\omega}$, we have an exact expression for the transition temperature

$$T_c = \left(\frac{\omega_0}{2\omega}\right) \frac{1}{\tanh^{-1}\left(\frac{\omega\omega_0}{(g_1+g_2)^2}\right)}. \tag{A10}$$

APPENDIX B: ROBUTSTNESS OF OUR RESULTS AGAINST INCREASING BOSONIC CUTOFF

In Fig. 7 we show the data corresponding to the ES-QPT and ENET for 20 spins and considering gradually increasing values of the bosonic truncation number $n_{\max} = 200, 300, 400, 500, 600$ (panels 1 to 5, respectively) to check the robustness of our results. In each panel of this figure, we show χ_{lower} (the lower cutoff energy which is scaled by the minimum energy in the nornal phase), χ_{upper} (upper cutoff energy which is scaled by the maximum energy at $g_1 = g_2 = 0$), consecutive level spacing ratio $\langle r \rangle$, participation ratio (PR), and the multifractal dimension (D_1) of the middle excited state, respectively, as a function of the coupling parameters g_1 and g_2. We notice that the results are qualitatively unchanged against increasing values of the bosonic truncation number $n_{\max}$ and are also converging.

[1] R. H. Dicke, Coherence in spontaneous radiation processes, Phys. Rev. **93**, 99 (1954).

[2] N. Lambert, C. Emary, and T. Brandes, Entanglement and the Phase Transition in Single-Mode Superradiance, Phys. Rev. Lett. **92**, 073602 (2004).

[3] C. Emary and T. Brandes, Chaos and the quantum phase transition in the Dicke model, Phys. Rev. E **67**, 066203 (2003).

[4] C. Emary and T. Brandes, Quantum Chaos Triggered by Precursors of a Quantum Phase Transition: The Dicke Model, Phys. Rev. Lett. **90**, 044101 (2003).

[5] E. Kadantseva, W. Chmielowski, and A. Shumovsky, Superradiance in the Dicke model, in *Nonlinear Optics in Solids* (Springer, New York, 1990), pp. 37–41.

[6] J. Chávez-Carlos, M. A. Bastarrachea-Magnani, S. Lerma-Hernández, and J. G. Hirsch, Classical chaos in atom-field systems, Phys. Rev. E **94**, 022209 (2016).

[7] P. Kirton and J. Keeling, Superradiant and lasing states in driven-dissipative Dicke models, New J. Phys. **20**, 015009 (2018).

[8] P. Kirton, M. M. Roses, J. Keeling, and E. G. Dalla Torre, Introduction to the Dicke model: From equilibrium to nonequilibrium, and vice versa, Adv. Quantum Technol. **2**, 1800043 (2019).

[9] M. Prasad, H. K. Yadalam, C. Aron, and M. Kulkarni, Dissipative quantum dynamics, phase transitions, and non-hermitian random matrices, Phys. Rev. A **105**, L050201 (2022).

[10] P. Das and A. Sharma, Revisiting the phase transitions of the Dicke model, Phys. Rev. A **105**, 033716 (2022).

[11] D. Yamamoto, C. Suzuki, G. Marmorini, S. Okazaki, and N. Furukawa, Quantum and Thermal Phase Transitions of the Triangular SU(3) Heisenberg Model under Magnetic Fields, Phys. Rev. Lett. **125**, 057204 (2020).

[12] T. Brandes, Excited-state quantum phase transitions in Dicke superradiance models, Phys. Rev. E **88**, 032133 (2013).

[13] M. A. Bastarrachea-Magnani, S. Lerma-Hernández, and J. G. Hirsch, Comparative quantum and semiclassical analysis of atom-field systems. i. density of states and excited-state quantum phase transitions, Phys. Rev. A **89**, 032101 (2014).

[14] P. Stránský and P. Cejnar, Classification of excited-state quantum phase transitions for arbitrary number of degrees of freedom, Phys. Lett. A **380**, 2637 (2016).

[15] P. Stránský, M. Kloc, and P. Cejnar, Excited-state quantum phase transitions and their manifestations in an extended Dicke model, in *Nuclei and Mesoscopic Physics 2017*, AIP Conf. Proc. No. 1912 (AIP, Melville, NY, 2017), p. 020018.

[16] P. Cejnar, P. Stránský, M. Macek, and M. Kloc, Excited-state quantum phase transitions, J. Phys. A: Math. Theor. **54**, 133001 (2021).

[17] H. Carmichael, C. Gardiner, and D. Walls, Higher order corrections to the Dicke superradiant phase transition, Phys. Lett. A **46**, 47 (1973).

[18] Y. K. Wang and F. T. Hioe, Phase transition in the Dicke model of superradiance, Phys. Rev. A **7**, 831 (1973).

[19] G. C. Duncan, Effect of antiresonant atom-field interactions on phase transitions in the Dicke model, Phys. Rev. A **9**, 418 (1974).

[20] M. A. Bastarrachea-Magnani, A. Relaño, S. Lerma-Hernández, B. L. del Carpio, J. Chávez-Carlos, and J. G. Hirsch, Adiabatic invariants for the regular region of the Dicke model, J. Phys. A: Math. Theor. **50**, 144002 (2017).

[21] D. Rubeni, A. Foerster, E. Mattei, and I. Roditi, Quantum phase transitions in bose–einstein condensates from a Bethe ansatz perspective, Nucl. Phys. B **856**, 698 (2012).

[22] A. D. Greentree, C. Tahan, J. H. Cole, and L. C. Hollenberg, Quantum phase transitions of light, Nat. Phys. **2**, 856 (2006).

[23] K. Stranius, M. Hertzog, and K. Börjesson, Selective manipulation of electronically excited states through strong light–matter interactions, Nat. Commun. **9**, 2273 (2018).

[24] J. Zhou, B. Huang, Z. Yan, and J.-C. G. Bünzli, Emerging role of machine learning in light-matter interaction, Light Sci. Appl. **8**, 84 (2019).

[25] N. S. Mueller, Y. Okamura, B. G. Vieira, S. Juergensen, H. Lange, E. B. Barros, F. Schulz, and S. Reich, Deep strong light–matter coupling in plasmonic nanoparticle crystals, Nature (London) **583**, 780 (2020).

[26] F. T. Hioe, Phase transitions in some generalized Dicke models of superradiance, Phys. Rev. A **8**, 1440 (1973).

[27] M. de Aguiar, K. Furuya, and M. C. Nemes, The classical analogue of the super-radiant phase transition in the

Dicke model, Quantum Opt.: J. Eur. Opt. Soc. Part B **3**, 305 (1991).
[28] M. de Aguiar, K. Furuya, C. Lewenkopf, and M. Nemes, Chaos in a spin-boson system: Classical analysis, Ann. Phys. (NY) **216**, 291 (1992).
[29] K. Furuya, M. de Aguiar, C. Lewenkopf, and M. Nemes, Husimi distributions of a spin-boson system and the signatures of its classical dynamics, Ann. Phys. (NY) **216**, 313 (1992).
[30] M. A. Bastarrachea-Magnani, S. Lerma-Hernández, and J. G. Hirsch, Thermal and quantum phase transitions in atom-field systems: A microcanonical analysis, J. Stat. Mech.: Theory Exp. (2016) 093105.
[31] W. Buijsman, V. Gritsev, and R. Sprik, Nonergodicity in the Anisotropic Dicke Model, Phys. Rev. Lett. **118**, 080601 (2017).
[32] M. Kloc, P. Stránský, and P. Cejnar, Quantum phases and entanglement properties of an extended Dicke model, Ann. Phys. (NY) **382**, 85 (2017).
[33] I. Aedo and L. Lamata, Analog quantum simulation of generalized Dicke models in trapped ions, Phys. Rev. A **97**, 042317 (2018).
[34] D. S. Shapiro, W. V. Pogosov, and Y. E. Lozovik, Universal fluctuations and squeezing in a generalized Dicke model near the superradiant phase transition, Phys. Rev. A **102**, 023703 (2020).
[35] J. Hu and S. Wan, Out-of-time-ordered correlation in anisotropic Dicke model, Commun. Theor. Phys. **73**, 125703 (2021).
[36] K. Baumann, R. Mottl, F. Brennecke, and T. Esslinger, Exploring Symmetry Breaking at the Dicke Quantum Phase Transition, Phys. Rev. Lett. **107**, 140402 (2011).
[37] U. Bhattacharya, S. Dasgupta, and A. Dutta, Exploring chaos in the Dicke model using ground-state fidelity and loschmidt echo, Phys. Rev. E **90**, 022920 (2014).
[38] P. Pérez-Fernández and A. Relaño, From thermal to excited-state quantum phase transition: The Dicke model, Phys. Rev. E **96**, 012121 (2017).
[39] S. Ashhab, Y. Matsuzaki, K. Kakuyanagi, S. Saito, F. Yoshihara, T. Fuse, and K. Semba, Spectrum of the Dicke model in a superconducting qubit-oscillator system, Phys. Rev. A **99**, 063822 (2019).
[40] R. J. Lewis-Swan, A. Safavi-Naini, J. J. Bollinger, and A. M. Rey, Unifying scrambling, thermalization and entanglement through measurement of fidelity out-of-time-order correlators in the Dicke model, Nat. Commun. **10**, 1581 (2019).
[41] J. H. Bardarson, F. Pollmann, and J. E. Moore, Unbounded Growth of Entanglement in Models of Many-Body Localization, Phys. Rev. Lett. **109**, 017202 (2012).
[42] S. Bera, H. Schomerus, F. Heidrich-Meisner, and J. H. Bardarson, Many-Body Localization Characterized from a One-Particle Perspective, Phys. Rev. Lett. **115**, 046603 (2015).
[43] N. Roy and A. Sharma, Entanglement contour perspective for "strong area-law violation" in a disordered long-range hopping model, Phys. Rev. B **97**, 125116 (2018).
[44] R. Nehra, D. S. Bhakuni, S. Gangadharaiah, and A. Sharma, Many-body entanglement in a topological chiral ladder, Phys. Rev. B **98**, 045120 (2018).
[45] D. P. DiVincenzo, M. Horodecki, D. W. Leung, J. A. Smolin, and B. M. Terhal, Locking Classical Correlations in Quantum States, Phys. Rev. Lett. **92**, 067902 (2004).
[46] X.-M. Lu, J. Ma, Z. Xi, and X. Wang, Optimal measurements to access classical correlations of two-qubit states, Phys. Rev. A **83**, 012327 (2011).
[47] L. Henderson and V. Vedral, Classical, quantum and total correlations, J. Phys. A: Math. Gen. **34**, 6899 (2001).
[48] G. Adesso and A. Datta, Quantum versus Classical Correlations in Gaussian States, Phys. Rev. Lett. **105**, 030501 (2010).
[49] G. M. H. Roósz, U. Divakaran, H. Rieger, and F. Iglói, Nonequilibrium quantum relaxation across a localization-delocalization transition, Phys. Rev. B **90**, 184202 (2014).
[50] J. Sirker, M. Maiti, N. Konstantinidis, and N. Sedlmayr, Boundary fidelity and entanglement in the symmetry protected topological phase of the ssh model, J. Stat. Mech.: Theory Exp. (2014) P10032.
[51] J. Cho and K. W. Kim, Quantum phase transition and entanglement in topological quantum wires, Sci. Rep. **7**, 2745 (2017).
[52] Z. Ma, Z. Chen, and F. F. Fanchini, Multipartite quantum correlations in open quantum systems, New J. Phys. **15**, 043023 (2013).
[53] A. Sharma and E. Rabani, Landauer current and mutual information, Phys. Rev. B **91**, 085121 (2015).
[54] H. S. Sable, D. S. Bhakuni, and A. Sharma, Landauer current and mutual information in a bosonic quantum dot, J. Phys.: Conf. Ser. **964**, 012007 (2018).
[55] K. Hepp and E. H. Lieb, On the superradiant phase transition for molecules in a quantized radiation field: The Dicke maser model, Ann. Phys. (NY) **76**, 360 (1973).
[56] Z. Chang, Generalized holstein-primakoff transformation, spin-charge separation and quantum nonlinear σ model in a 2d lattice, Phys. Lett. A **204**, 405 (1995).
[57] E. Ressayre and A. Tallet, Holstein-primakoff transformation for the study of cooperative emission of radiation, Phys. Rev. A **11**, 981 (1975).
[58] J. T. Edwards and D. J. Thouless, Numerical studies of localization in disordered systems, J. Phys. C **5**, 807 (1972).
[59] N. Roy, A. Ramachandran, and A. Sharma, Interplay of disorder and interactions in a flat-band supporting diamond chain, Phys. Rev. Res. **2**, 043395 (2020).
[60] P. Pérez-Fernández, A. Relaño, J. M. Arias, P. Cejnar, J. Dukelsky, and J. E. García-Ramos, Excited-state phase transition and onset of chaos in quantum optical models, Phys. Rev. E **83**, 046208 (2011).
[61] S. A. Hill and W. K. Wootters, Entanglement of a Pair of Quantum Bits, Phys. Rev. Lett. **78**, 5022 (1997).
[62] W. K. Wootters, Entanglement of Formation of an Arbitrary State of Two Qubits, Phys. Rev. Lett. **80**, 2245 (1998).
[63] Y. Y. Atas, E. Bogomolny, O. Giraud, and G. Roux, Distribution of the Ratio of Consecutive Level Spacings in Random Matrix Ensembles, Phys. Rev. Lett. **110**, 084101 (2013).
[64] A. Kamenev and M. Mézard, Wigner-dyson statistics from the replica method, J. Phys. A: Math. Gen. **32**, 4373 (1999).
[65] N. Macé, F. Alet, and N. Laflorencie, Multifractal Scalings Across the Many-Body Localization Transition, Phys. Rev. Lett. **123**, 180601 (2019).
[66] J. Lindinger, A. Buchleitner, and A. Rodríguez, Many-Body Multifractality throughout Bosonic Superfluid and Mott Insulator Phases, Phys. Rev. Lett. **122**, 106603 (2019).
[67] H. Jeffreys, B. Jeffreys, and B. Swirles, *Methods of Mathematical Physics* (Cambridge University Press, Cambridge, England, 1999).